Wave-Follower Field Measurements of the Wind-Input Spectral Function. Part I: Measurements and Calibrations

MARK A. DONELAN

Rosenstiel School of Marine and Atmospheric Science, University of Miami, Miami, Florida

ALEXANDER V. BABANIN

School of Engineering and Science, Swinburne University of Technology, Melbourne, Victoria, Australia

IAN R. YOUNG

Swinburne University of Technology, Melbourne, Victoria, Australia

MICHAEL L. BANNER

School of Mathematics, University of New South Wales, Sydney, New South Wales, Australia

CYRIL MCCORMICK

Rosenstiel School of Marine and Atmospheric Science, University of Miami, Miami, Florida

(Manuscript received 19 August 2002, in final form 27 July 2004)

ABSTRACT

An experimental study of wind energy and momentum input into finite-depth wind waves was undertaken at Lake George, New South Wales, Australia. To measure microscale oscillations of induced pressure above surface waves, a high-precision wave-follower system was developed at the University of Miami, Florida. The principal sensing hardware included Elliott pressure probes, hot-film anemometers, and Pitot tubes. The wave-follower recordings were supplemented by a complete set of relevant measurements in the atmospheric boundary layer, on the surface, and in the water body. This paper is dedicated to technical aspects of the measurement procedure and data analysis. The precision of the feedback wave-following mechanism did not impose any restrictions on the measurement accuracy in the range of wave heights and frequencies relevant to the problem. Thorough calibrations of the pressure transducers and moving Elliott probes were conducted. It is shown that the response of the air column in the connecting tubes provides a frequency-dependent phase shift, which must be accounted for to recover the low-level induced pressure signal. In the finite-depth environment of Lake George, breaking waves play an important role in the momentum exchange between wind and waves, as will be shown in a subsequent paper.

1. Introduction

Spectral evolution of the wind-generated wave field is commonly described by the radiative transfer equation (Hasselmann 1960):

$$\frac{dF(\omega, \mathbf{k})}{dt} = I(\omega, \mathbf{k}) + N(\omega, \mathbf{k}) + D(\omega, \mathbf{k}), \qquad (1)$$

where the total derivative of the frequency–wavenumber spectrum $F(\omega, \mathbf{k})$ on the left-hand side is balanced by the sum of energy source I, sinks D, and spectral redistribution N terms on the right. Here, only energy terms for wind input I, dissipation in the water column D, and four-wave nonlinear interactions N are mentioned, as they are usually the dominant terms. Equation (1) is the basic equation used in most phase-averaged numerical wave prediction models (Sobey 1986).

The wind-input source term $I(\omega, \mathbf{k})$ is the subject of the present paper. It is always of primary importance in

Corresponding author address: Dr. Alex Babanin, School of Engineering and Science, Swinburne University of Technology, Melbourne, VIC 3122, Australia.
E-mail: ababanin@swin.edu.au

wave evolution models since it is responsible for generation and sustenance of the wave fields. Unlike the other "source" terms, the spectral wind input I can be directly measured. The major part of the momentum transfer from the turbulent wind into surface waves is due to wind pressure pulsations correlated with the water surface slope. Therefore, synchronous measurement of these pulsations and the water surface elevation provides estimates of the growth increment $\gamma(\omega, \mathbf{k})$ and, once the wave spectrum $F(\omega, \mathbf{k})$ is known, of the wind-input function $I(\omega, \mathbf{k})$ (mathematical definitions are given in section 3).

However, there are numerous difficulties associated with this type of measurement. The pressure variations of interest are of order 10^{-5} to 10^{-4} of the mean atmospheric pressure (Young 1999), which means that very sensitive pressure probes have to be used. In this small pressure signal, the aim is to measure small (often just a few degrees) phase differences from 180°between the pressure and the surface elevation. This imposes very strict requirements on the precision of all records, both in space and time. Since the pressure exerted directly on the water surface is required, the measurements must be carried out as close to the surface as possible, ideally at the surface itself. Air pressure fluctuations induced by the waves decay very quickly with height, and if the measurements are performed at a fixed level above the dominant wave crests, most information about the interaction at higher frequencies, that is, about spectral distribution of the wind input, is lost.

The probes, sensing pressure in the air, need to stay dry, and therefore they must be mounted on a wave-following system to be able to conduct measurements below the wave crests. It is also necessary to follow the water surface in order to keep the probes at a constant height above the water, which is needed to account for the height decay of induced pressure variations. The wave following, however, introduces a new problem for subsequent data analysis: as the pressure probe moves, additional pressure terms are induced due to displacement and acceleration of the probe and movement of air in the tubes connecting the probe and the transducer.

In field conditions the above-mentioned difficulties are exacerbated by uncertainties of the measurements caused by directionality of the incoming waves and wind gusts: air pressure–surface slope correlation is now three-dimensional. Another serious drawback with field pressure measurements very close to the surface is that breaking waves can suddenly and unexpectedly overturn on a sensing probe or bring whitecapping to a probe's location and thus wet the probe and interrupt the recording. Furthermore, breaking rates in finite-depth environments, for example, are very high. In strong wind conditions, 60% of the dominant waves were recorded as breaking in a 20 m s^{-1} wind at Lake George (Babanin et al. 2001).

A number of devices and platforms have been previously designed to carry pressure probes for wind-input studies. The first measurements of this type were made by Longuet-Higgins et al. (1963), who used a large flat buoy as the following system. The measurements proved rather unsuccessful, as no significant phase difference from 180° between the pressure and the waves was reported. Dobson (1971) used a very small buoy to make an extensive series of observations and found values of wave growth increments β consistent with known wave growth rates. There are many problems associated with such buoy measurements. The smaller the buoy, the more frequently its vertical axis, carrying the pressure probe, is tilted relative to the incoming wind flow, unless some constraints are in place. However, the larger the buoy or the more constraints that are applied, the greater the potential distortion introduced into the airflow. Buoys are always larger than the pressure probes they carry, and therefore the resulting flow distortion reduces significantly the resolution capacity of the probes. Also, neither large nor small buoys can properly ride the surface of breaking waves, often leading to splashing of the probes.

As an alternative to the wave-following system, stationary arrays of pressure probes have been deployed. Elliott (1972b) used a vertical array of fixed air pressure sensors and found values of $\gamma \approx 0.2$, which is significantly lower than those of Dobson (1971), as well as slightly less rapid height decay of the induced air pressure field compared with potential theory. Snyder (1974) used a horizontal array of wave and fixed air pressure sensors to take into account directional properties of the wave and air pressure fields. His measured growth increments $\gamma \approx 0.1$ were even smaller than those reported by Elliott (1972b). A vertical array of stationary probes was also used by Hasselmann and Bösenberg (1991) in a later attempt to investigate atmospheric input in open ocean conditions. Their experiment produced $\gamma \approx 0.25$. An apparent disadvantage of the fixed array measurements is the fact that the probes must be operated above the highest wave crest to stay dry. This limits the results to dominant wave scales since the higher-frequency contributions of the induced pressure field are filtered out by the height decay. Furthermore, dealing with the pressure height decay becomes ambiguous because the distance of the array probes from the water surface is not constant. A possible advantage of measurements by a horizontal

array—estimating directional properties of γ—was never reliably realized, and the assumed (Plant 1982) directional function $\gamma(\omega, \theta) = \gamma(\omega)cos\theta$ is used in most models.

To reconcile the differences among the results of Dobson, Elliott and Snyder, a combined field experiment was conducted (Snyder et al. 1981) in the Bight of Abaco, Bahamas. Along with arrays of fixed probes, they introduced a specially designed wave follower that became a primary device for later wind-input studies. Various realizations of wave followers implement the same basic idea: a wave follower senses the local elevation of the moving water surface and produces vertical motion of the mounted pressure probes so that the probes are kept at a constant height above the surface. This allows one to maintain the air pressure sensors close to the water and thus extends the frequency band of resolvable pressure wave cross-spectra. The sensor orientation is held stable, and the probe is less likely to be swamped by a breaking wave. The drawbacks include the difficulties associated with deployment of the device: a rigid platform is needed to mount the usually rather large body of a follower, which is rarely available in field conditions, particularly at deep-water sites. Also, as has been mentioned above, the moving probe introduces contamination into the output pressure signal.

Use of wave followers has significantly increased the parameter range of the measurements and enhanced the precision. The Snyder et al. (1981) data spanned a broad spectral range around the spectral peak ($1 < U_{10}/c < 3$), and Hsiao and Shemdin (1983) in a subsequent North Sea field experiment extended it even further toward smaller scales ($1 < U_{10}/c < 7.4$). Here, U_{10} is the wind speed at standard 10-m height and $c = \omega/k$ is wave phase speed. The field experiments were followed by extensive and more accurate laboratory studies by Young and Sobey (1985) and Donelan (1999). However, there is still significant scatter in the values of the reported growth increment γ; parameterizations of γ are inconsistent with each other; and, most importantly, the measurements so far have not shed much light on the physical processes responsible for the wave-induced pressure and hence the nature of the energy input.

This paper describes a new field experiment dedicated to measurements of momentum and energy transfer from wind to waves in finite-depth water. Section 2 provides a detailed account of the experiment: its goals, description of the experimental site, instrumentation, and supplemental measurements. Section 3 sets up definitions of the measured quantities and discusses data processing: precision of the measurements, calibration procedures, corrections for the effects of moving probes (including important, though previously overlooked, concerns), methodology of the data analysis, cross-checks of the results with independently measured properties, and aspects of the Lake George finite-depth spectra. Conclusions are formulated in section 4. The second and third parts of the wind-input study, dedicated to physical results and parameterization of the wind input in terms of wind-wave field properties and the enhancement of the wind input due to wave breaking, will be published as separate papers.

2. The experiment

The Lake George experiment was designed to simultaneously measure the major wind-generated water wave source and sink functions in a finite-depth field environment (apart from the nonlinear interactions, which are to be computed). This paper considers the wind-input term only.

Direct measurement of the wind-input source function was one of the goals of the Lake George experiment. Apart from defining the total energy balance, accurate determination of the wind input is an important issue in its own right. Experimental knowledge of the wind-input parameterization is far from complete (see Young 1999), and field experiments can add valuable insight to the problem. Few such field experiments have been carried out in recent times, due to the technical difficulties in conducting these studies. As a result, experimental knowledge in this area lags behind theoretical advances. New theories of energy and momentum exchange are discussed in detail in the second part of the paper, and verification of them requires new experimental effort.

This study incorporated new technological advances and physical approaches. In the period since wave-following measurements were first attempted, there have been significant advances in technology (see Donelan 1999), and a new generation of wave followers allows more precise measurements to be made very close to the surface, in a wave-following coordinate system. Also, new understanding of the dynamic response and associated corrections required for such moving-probe measurements has come to light, which is described in this paper and significantly improves the accuracy of higher frequency measurements of the wind input.

An important issue, which has, to date, not been considered in wind-input parameterizations, is possible enhancement of the wind-wave momentum and energy exchange by breaking waves. Banner and Melville (1976) and Banner (1990) demonstrated clear effects of

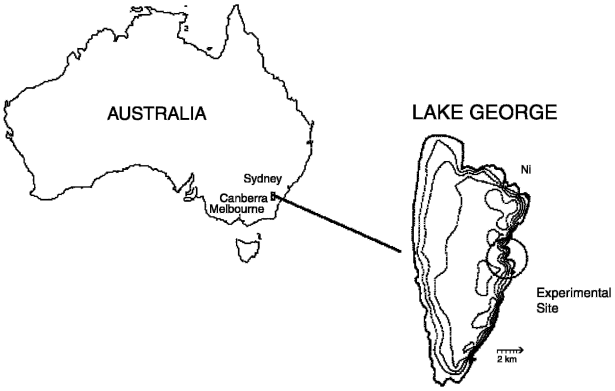

FIG. 1. Location of the Lake George site.

FIG. 2. The research platform is located in such a way that it is openly exposed to westerly and northwesterly winds, most common at Lake George.

airflow separation above breaking waves that can, according to Banner (1990), double the momentum exchange rate between the wind and the waves. To provide a possibility of isolating breaking wave effects and to study the wind-input enhancement due to breaking, the Lake George experiment was designed such that breaking waves were detected and recorded.

a. The experimental site

The Lake George field site was established and maintained for the period 1997–2000 near the eastern shore of Lake George, in New South Wales, Australia [Fig. 1, which is reproduced from Fig. 1 in Babanin et al. (2001)]. Measurements were conducted on the eastern shore of the lake, chosen because of the predominant west and northwest winds in the area, which provided the experiment with frequent well-developed wave conditions. A contour map of Lake George, shown in Fig. 1, indicates simple bathymetry, with the bed sloping very gently toward the eastern shore of the lake. Since the bed is extremely flat, Lake George is an ideal location to study in situ fetch-limited behavior of wind-generated waves in a near-constant, finite-depth environment. Due to seasonal variations, the water depths varied significantly within the 3-yr span, from a maximum of 1.12 m down to almost zero by the time the experiment was concluded in August 2000. In these depth-limited conditions, fetches of up to 8 km allowed the waves to reach a fully developed stage at the measurement site (see Young and Verhagen 1996a,b). For linear waves the experimental conditions were representative of intermediate-depth wind seas; that is, nondimensional depth $k_p d$ was $0.7 < k_p d < 3$.

The experimental site included an observational platform with a shelter to accommodate equipment and researchers during observational periods [Fig. 2, reproduced from Fig. 2 in Babanin et al. (2001), provides a general view]. The platform was located 50 m offshore and was accessible via an elevated walkway in any weather conditions. The measurements, relevant to the present paper, were made from a 10-m-long elevated bridge located to the side of the platform (see Fig. 2). A comprehensive instrumentation system was set up to carry out simultaneous measurements and recordings in the atmospheric boundary layer, on the water surface, in the water column below the surface, and at the bottom. All the devices, with the exception of the wave-following system described in the next subsection and the sonic anemometer, recorded data at a rate of 25 Hz and sampled in a synchronized mode. The sonic anemometer sampled data at a rate of 21 Hz, with its start time being synchronized to within 1 min with the rest of the instruments.

b. AUSWEX

The Australian Shallow Water Experiment (AUSWEX) was conducted in August and September 1999, when the mean water depth at the experimental site was about 40 cm. In addition to the above-mentioned instrument set, measurements in the atmospheric boundary layer very close to the water surface were carried out by means of a wave follower, designed at the University of Miami, Florida, and measurements of the spatial distributions of water turbulence were performed with the aid of a coherent acoustic Doppler ("Dopbeam") device provided by the Scripps Institution of Oceanography, California (Veron and Melville 1999).

The wave follower was the primary tool to enable direct measurements of the wind input. In Fig. 3a it is

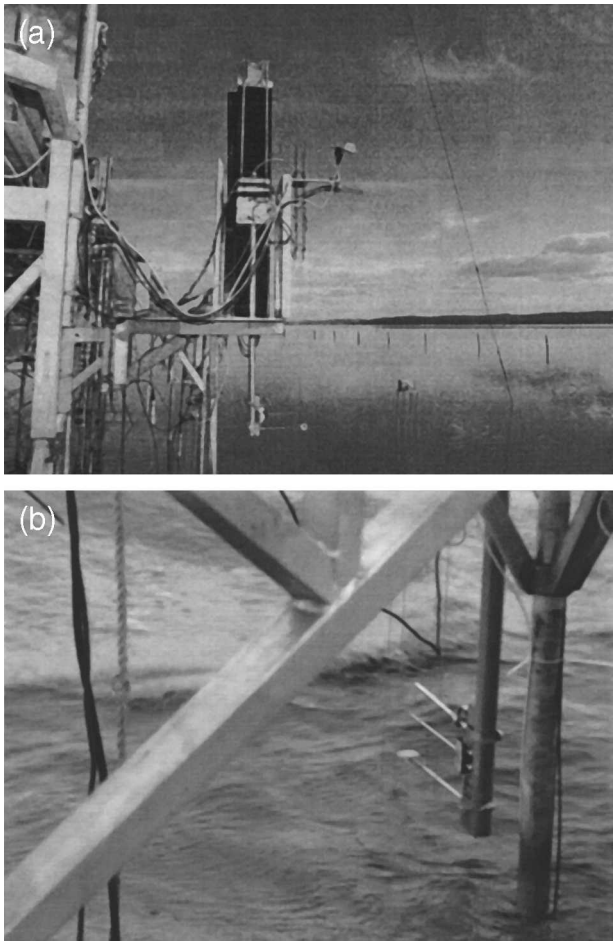

FIG. 3. (a) The wave follower, shown positioned on the measurement bridge during AUSWEX. (b) The bottom of the wave-follower shaft, while operational. Three fingers with pressure probes following a wave crest can be seen. The Elliott probe is at the bottom, with the hot-film anemometer above this and the Pitot tube at the top.

shown positioned on the measurement bridge during AUSWEX. As can be seen, the follower was installed on a special platform off the measurement bridge that could be rotated and thus allowed for changes in the orientation of the follower's probe so as to align it with the wind and wave directions. The signal from a resistance probe, consisting of a loop of wire with vertical arms separated by 10 cm, was used to determine the instantaneous position of the surface midway between the vertical arms, that is, in the same (x, y) position as the ports of the Elliott pressure disk (Elliott 1972a), which was constrained to move vertically by the wave follower. The loop was attached at the top to the platform and at the sediment/water interface to a plate, which was rigidly connected to the platform by a vertical pipe of 5.08-cm diameter (see Fig. 3a). The resistance of the wire loop is directly proportional to the exposed (out of the water) portion of the wire loop. An AC bridge, designed and built by the technicians at the Australian Defense Force Academy, was used to determine the resistance and hence the surface elevation. This is the signal that the wave follower was designed to follow. The feedback loop was closed by comparison of the surface elevation with the position of the "stage" of the vertical linear motor (Enclosed Positioning Stage, EPS 800–36, manufactured by Northern Magnetics). The feedback loop controls the velocity of the stage and acts to force the stage's position (i.e., the summed steps of 5 μm of the linear motor) to match the surface elevation. The digital feedback control is realized through the "DMC-1000 embedded control language" used to activate an AMC-PWM Servo amplifier, BE25420AC (manufactured by Northern Magnetics). Maximum achievable velocity and acceleration of the stage were 2 m s^{-1} and 25 m s^{-2}. Before each run, calibration of the resistance wire wave gauges was performed by winching the platform up and down over 40 cm. An example of the follower in operation is shown in Fig. 3b with an Elliott pressure disc at the bottom, a hot-film set directly above, and a Pitot tube at the top.

In addition to the surface elevation and the three following probe signals, the wave-follower system also recorded data from an array of three capacitance wire wave gauges, a stationary hot-x-film set, located on the wave-follower body above the bridge, a set of three bottom-mounted pressure probes (located at the footprint of the follower, providing both directional wave information and detection of the breaking events, as well as mean position of the water surface); a hydrophone mounted at the bottom under the measurement point and designed to sense the vertically propagating acoustic noise due to passing breaking waves; a wind vane with instantaneous values of the wind direction. The position of the wave follower was also recorded to provide an additional check of the accuracy to which the follower tracked the water surface.

The wave-follower instrumentation sampling frequency was 50 Hz, twice the rate of the other instrumentation. To synchronize the two independent measurement systems, a sawtooth signal was generated and recorded by both the wave follower and the main logging computer. When operating in the following mode, the wave follower and the water surface were videotaped at the rate of 25 frames per second. The frames were also synchronized with the other measurements.

c. Other wave and atmospheric measurements

The main wave-measuring device at the site was a capacitance wave array of eight gauges, located ap-

proximately halfway along the bridge. Three more mobile arrays were also used: two single-probe capacitance gauges and a three-probe resistance array. The mobile arrays were positioned on the shallow bottom, at varying distances and orientations relative to the main stationary array. These gauges were deployed to provide information on the advection properties of the wave field, transformation of wave groups, and changes in the wave properties due to wave breaking. Average breaking wave statistics were collected with a hydrophone, collocated with the stationary wave array (see Babanin et al. 2001).

For flux measurements in the atmospheric boundary layer, an anemometer mast, accommodating three wind probes at 10- and 5.65-m elevations above the surface (two cup anemometers and one wind vane) was erected 10 m from the platform beyond the end of the measurement bridge to avoid disturbing the airflow. Another anemometer mast, accommodating five wind probes at four heights closer to the surface (four cup anemometers and a wind vane), was located 6 m to the side of the bridge (Fig. 2) to ensure undisturbed airflow for these lower anemometers. Thus, the two masts measured 1-min averages of the wind profile with instruments spaced logarithmically throughout the lower 10 m of the boundary layer.

A sonic anemometer recorded fluctuations of the airflow in the three spatial directions. This instrument was located at the top of the second anemometer mast during AUSWEX. Its position, far from all the structures, provided for free airflow, necessary for high-accuracy turbulence measurements, and also provided an additional point measurement for the determination of boundary layer wind profiles. The humidity and air and water temperatures were also synchronously recorded.

3. Data processing

It is known that the component of pressure that is correlated with the water surface slope, or, as it is often termed, the component of pressure in quadrature with the water surface, will result in an energy flux to the waves (see, e.g., Donelan 1999; Young 1999):

$$\frac{\partial E(\omega)}{\partial t} = \frac{1}{\rho_w g} I(\omega) = \frac{1}{\rho_w g} \overline{p \frac{\partial \eta}{\partial t}} = \frac{1}{\rho_w g} \overline{p \frac{\partial \eta}{\partial x}} \cdot c(\omega). \tag{2}$$

Here, $E(\omega) = \int_{\mathbf{k}} F(\omega, \mathbf{k})\, d\mathbf{k}$ is the one-dimensional frequency spectrum, which will be primarily dealt with in this paper; $I(\omega)$ is the corresponding one-dimensional frequency function of the wind input [we keep the same symbol, as in Eq. (1), for simplicity]; ρ_w is the water density; g is the gravitational constant; p is the pressure exerted by the air on the surface; $\eta(x, t) = a \cos(kx - \omega t)$ is the surface elevation; and $c(\omega)$ is the phase speed. The overbar represents an average with respect to time.

The nondimensional growth rate is customarily expressed in terms of the fractional energy increase per radian, γ:

$$\gamma(\omega) = \frac{\rho_w}{\rho_a} \frac{1}{\omega E(\omega)} \frac{\partial E(\omega)}{\partial t}. \tag{3}$$

Here, ρ_a is the density of air. Equations (2) and (3) lead to

$$\gamma(\omega) = \frac{Q(w)}{\rho_a g E(\omega)} \tag{4}$$

(Snyder et al. 1981), where

$$Q(\omega) = \langle p(\omega)\eta(\omega)^* \rangle \tag{5}$$

is the quadrature spectrum between the exerted pressure p and the surface elevation η, and the brackets mean the ensemble averaging in Fourier space. The asterisk (*) refers to the complex conjugate.

As far as direct experimental measurements of the wind input are concerned, the goal is to accurately estimate the quadrature spectrum $Q(\omega)$ based on simultaneous recordings of the surface elevation and the surface pressure at a point on the surface. In the present study, the input function properties will be routinely interpreted in terms of the nondimensional ratio of $Q(\omega)$ to the wave energy, termed the fractional growth rate $\gamma(\omega)$ as described by (4). Once the growth rate function $\gamma(\omega)$ is known and the power spectrum $E(\omega)$ is available, the dimensional wind input is

$$I(\omega) = \rho_a \omega g \gamma(\omega) E(\omega). \tag{6}$$

a. Measurements of the quadrature spectrum

A wave follower, described above (Fig. 3), was the device employed to enable measurements of the quadrature spectrum (5). The time series of surface variation were recorded in two ways: as surface elevations measured by the resistance wave probe and as the stage position of the vertical position of the follower's arm, which was meant to follow the water surface precisely, and therefore the wave probe signal. Since the resistance wire characteristics were inclined to drift, calibrations of the resistance probes were performed before each run. The calibration curves were linear for all practical purposes and allowed measurements of surface elevations with 1-mm accuracy, which was beyond the necessary accuracy limits for wave measurements in the frequency range of interest.

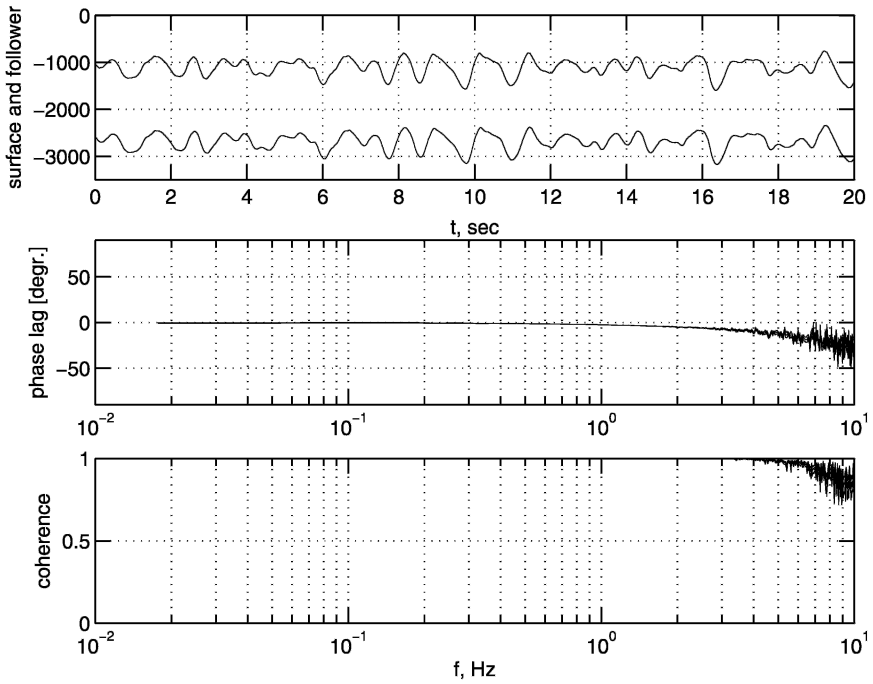

FIG. 4. Comparison of the surface elevation and wave-follower stage position: (top) fragment of a time series (elevation is the top line, units are arbitrary); (middle) phase lag (negative shift means the stage lags the wave); and (bottom) coherence of the two signals.

Coherence and phase shift between the surface elevation and the stage position are shown in Fig. 4. As can be seen, the coherence is very high all across the spectrum and is essentially unity up to about 6 Hz. Note that 4 Hz was the maximum frequency for the measured quadrature spectrum, because of the rapid height decay of the wave-induced pressure signal, as described below. The phase lag is less than 10° in the frequency range of interest (0.1–4 Hz). Confidence intervals for the coherence and phase estimates are so small that they cannot be discerned on a linear scale. As an example, we can mention that at the peak frequency (0.76 Hz for the record shown in Fig. 4), coherence and its 95% confidence limits were $0.999\,997\,0^{+0.000\,000\,9}_{-0.000\,001\,2}$, and phase lag and its 95% confidence limits were $-1.852° \pm 0.022°$.

The wave-induced pressure and velocity oscillations were measured by three sensors located on the moving follower arm at a constant height above the surface (see Fig. 3b). Closest to the surface was the Elliott probe, which measured the induced pressure. The size of the Elliott probe, 4 cm in diameter, imposed limitations on the pressure fluctuations registered, upperbound at approximately 6 Hz. The hot film and Pitot tube, respectively 10 and 15 cm above the Elliott probe, provided a direct measure of the Reynolds stress as well as the wave coherent horizontal and vertical velocity components. All pressure measurements were made with model "223BD Baratron" differential pressure transducers manufactured by MKS Instruments. These transducers operate on variable capacitance principle, in which the pressure-induced motion of a tensioned metal diaphragm alters the capacitance between the diaphragm and a fixed electrode. The diameter of the diaphragm is 6 cm, and the internal volume of the instrument on the measuring side is 1.3 cm^3 and on the reference side is 9.8 cm^3. The instruments have a resolution of 0.01% of full scale and an accuracy of 0.5% of full scale. Laboratory calibrations performed before and after the field campaign verify the stability of the instruments to the stated accuracy. The limiting resolution was the quantization error of the 12-bit A/D system (0.024%) used to record all analog instruments. The Elliott and Pitot probes were connected to transducers with full-scale ranges of ±5 V, corresponding to ±0.5 in. of water. The expected maximum signals were 0.2 and 0.47 in. of water (50 and 117 Pa) for the Elliott and Pitot probes, respectively, in a 14 $m\,s^{-1}$ wind with waves of slope 0.2. Ultimately, the fidelity of the wave-induced pressure measurements depends on the ability of the Elliott probe to reject contamination of the actual pressure by pressure induced by the flow around the probe. This probe shape has been shown to have a pressure coefficient of less than 0.01 in the pitch angle

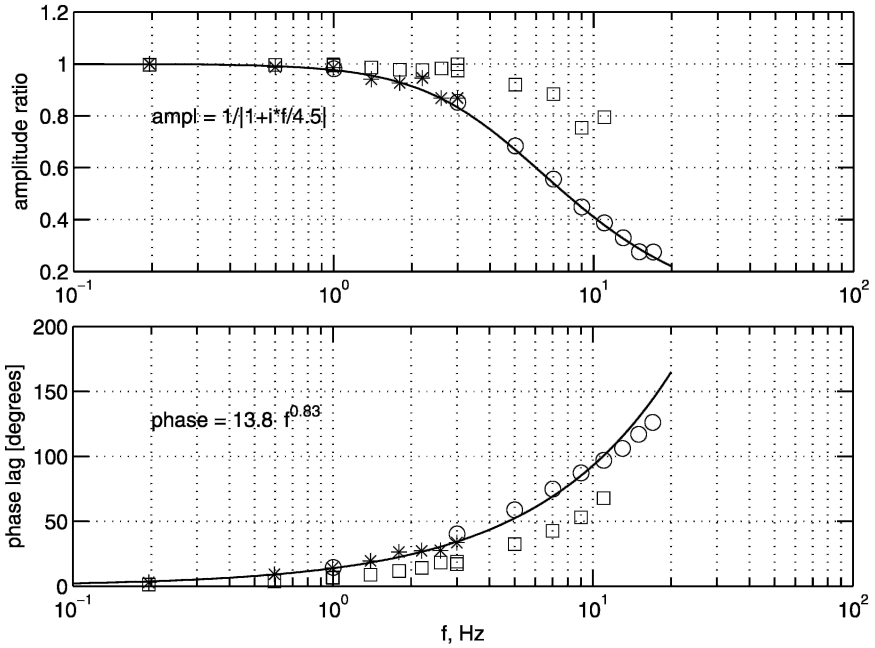

FIG. 5. Calibration curves of the pressure transducer. Asterisks (*) correspond to the 0.2-Hz triangular sound wave at the entrance; open circles (o) correspond to the 1-Hz wave at the end of AUSWEX; and open squares show calibration measurements prior to AUSWEX. Positive phase shift means the input pressure leads the transducer response.

range of ±10° (Elliott 1972a; Snyder et al. 1981). Of course, the symmetry of the probe about a vertical axis ensures its insensitivity to horizontal variations in the wind direction.

Therefore, the wave-follower/pressure system was capable of accurately detecting signals that are necessary to estimate the quadrature spectrum or the spectral wind input from the low-frequency end of the wind-wave band through to 4–6 Hz. It is the highest-precision wave-following system yet used in field conditions.

b. Corrections to the pressure signal

To realize the high-precision capacity of the follower to measure the quadrature spectrum, multiple corrections have to be applied to the recorded pressure signal. Whereas after correction for the wave-follower response function there is no difference between the sensed and recorded surface elevations, differences between the detected pressure and applied pressure are significant. These differences are caused by the fact that the pressure at the inlet orifice of the Elliott probe is not immediately converted into an electric signal but undergoes various stages of transformation before being sensed by the pressure transducer. Also, the pressure is not measured at the water surface, where it is meant to be exerted, according to (5), but at some height above this, and therefore requires extrapolation to the surface in order to estimate the wind input.

1) CALIBRATION OF THE PRESSURE TRANSDUCER

The first correction to be made relates to the static (i.e., assuming no motion of the wave follower) transfer function of the system comprising the Elliott probe, MKS pressure transducer, and connecting tubing. This correction allows one to convert the recorded pressure signal (voltages from the MKS transducer recorded by the wave-follower logging system) into calibrated and phase-corrected air pressure at the entrance of the transducer. The reference or backup volume was sealed for AUSWEX.

The static transfer function was obtained by means of a sound generator (radio speaker) applied at one end of a closed cylinder with the Elliott probe inside. The speaker was activated by a signal generator using triangular waveforms of two different frequencies: 0.2 and 1 Hz in turn. Hence, the speaker applied a known pressure signal to the closed volume, which was measured by the probe, connecting tubing, and transducer system. The response of the transducer to such a signal, decomposed in Fourier space, is shown in Fig. 5. As seen in the figure, the amplitude response was parameterized as an RC filter function and the phase response as an exponential function. The parameterizations were then used

to recover the pressure signal transmitted through the Elliott probe and connecting tubing at the entrance of the pressure transducer. [See Donelan et al. (1999) for more details.]

The response properties of the system are dependent on the resistance to flow through the ports of the Elliott probe. This changed slowly over time due to natural contamination by moisture and dust, and to account for this a number of calibrations were performed during AUSWEX. In times between the calibrations, the probe frequency responses were interpolated linearly. Figure 5 shows calibration points measured before and after AUSWEX and the calibration fit for the latter.

Static calibrations of the pressure transducers used at Lake George were repeated in the laboratory at the Center for Air–Sea Interaction (CASI), Rosenstiel School of Marine and Atmospheric Science (RSMAS), University of Miami, Florida, 1 yr after AUSWEX in October 2000, and the calibration coefficients were confirmed to stay virtually unchanged. This was done to make use of the Elliott probe with the same calibrations, as at Lake George, for further laboratory testing of pressure-to-acceleration responses, as described in section 3b(2).

2) CORRECTION FOR THE ACCELERATION OF THE SENSOR AND TUBING

The correction for the static response of the pressure transducer [described in section 3b(1)] is an important part of the data processing and requires fine, accurate, and regular calibrations. It is well understood and has been established and routinely performed in similar wind-input studies. On the other hand, the correction for the wave follower's acceleration of the column of air between the Elliott pressure probe and the diaphragm of the pressure transducer is somewhat more delicate.

In previous studies the pressure imposed by acceleration of the air in connecting tubes of length h was assumed to be a function of the second derivative of the sensor's vertical displacement z [i.e., the vertical acceleration; see, e.g., Snyder et al. (1981)]:

$$p_a = \frac{1}{2}\rho_a h \frac{d^2 z}{dt^2}. \tag{7}$$

While this is appropriate for a closed column of air, the "leakage" of air through the pressure probe may lead to a more complicated response. During AUSWEX, the connecting tubes were 1.28 m long, and the pressure due to the acceleration term was significant, and the induced phase shift needed to be measured accurately.

To do so, a series of laboratory tests was performed at CASI with the Lake George wave-following system configuration: the same follower, the same Elliott probe and pressure transducer [with confirmed same calibrations; see section 3b(1)], and the same tubes connecting them. The wave follower was positioned horizontally (in order to avoid gravitational effects of the stage displacement on the pressure), and sinusoidal waves of different frequencies and amplitudes were fed to the motor to oscillate the air column and register the acceleration-induced pressure response. Different connecting tube lengths were also used. The acceleration was independently measured by an accelerometer.

A set of the pressure-to-acceleration responses is shown in Fig. 6 for the same tube length [configuration with the Elliott probe having both orifices open (x) corresponds to the configuration used during AUSWEX]. This figure shows frequency responses for open- and closed-end situations, as well as situations with the Elliott probe attached. Clearly, along with the amplitude dependence, the phase lag between the pressure and the acceleration is not a constant across the frequency band. This implies very significant consequences for the conversion of the pressure signal, as is shown in Fig. 7. The resulting acceleration-to-induced pressure transfer function is shown in Fig. 6 by a continuous line fitted to the x-marked Elliott configuration curve. Confidence intervals for the amplitude and phase frequency responses are very small and not discernible on this plot. At 0.76-Hz frequency, the amplitude and its 95% confidence limits were $0.7859 \pm 0.000\,35$, and phase lag and its 95% confidence limits were $-168.76° \pm 0.025°$.

The transfer function was used to recover the real pressure at the Elliott probe entrance, and an example of the outcome is shown in Fig. 7. The correction yields significant differences. Acceleration for the field records was obtained by means of double differentiation of the wave signal from the resistance probe with a minor amplitude and phase adjustment to account for the measured wave-follower response (see Fig. 4). Given the very high sampling rate (50 Hz), uncertainty due to the numerical double differentiation in the frequency range of interest (up to 4 Hz) is negligible.

During the Lake George record, shown in Fig. 7, the Elliott pressure sensor was kept at 5 cm above the moving water surface, and one can hardly expect any pressure signal above 3 Hz to be coherent with the surface because of the rapid height attenuation of the wave-induced pressure signal. Figures 7a and 7b show the phase lag and coherence between the surface-elevation record and the Elliott-measured pressure signal corrected for acceleration of the probe as in (7). The coherence quickly drops above the spectral peak, which is at $f_p = 0.6$ Hz for this case, and then rises rapidly at

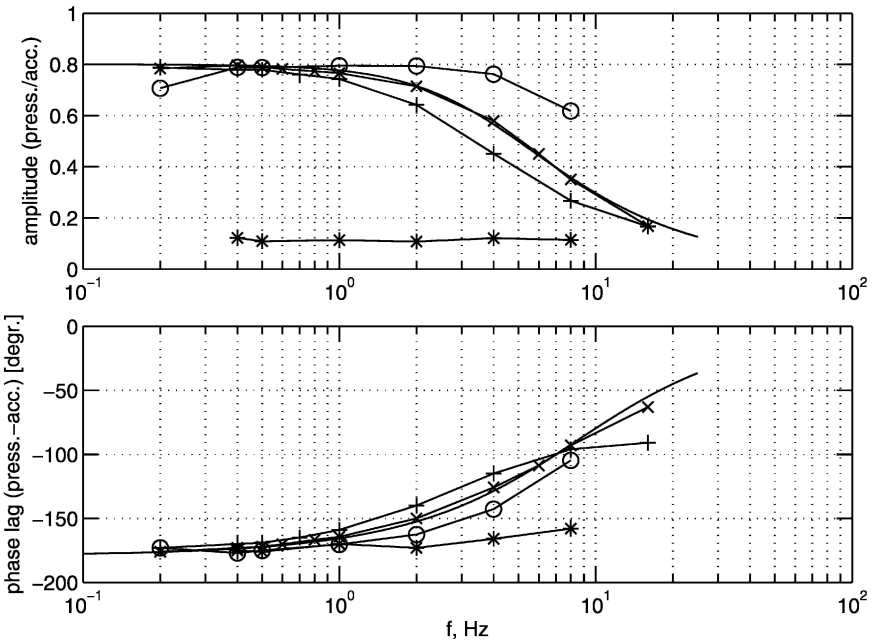

FIG. 6. Frequency dependence of pressure, induced by acceleration of the air column in the connecting tubes. (o)—open end; (x)—Elliott probe end (AUSWEX configuration); (+)—Elliott probe, with one orifice closed; and (*)—closed end. The transfer function is shown with a smooth line fitted to the x-marked dependence. Negative phase shift means the pressure lags the acceleration.

frequencies $f > 1$ Hz; the values above 2 Hz are clearly spurious. In Figs. 7c and 7d the correction is made based on the laboratory-measured acceleration-induced term, as in Fig. 6. The coherence stays level up to at least 2 Hz, and only approaches the spurious values of Fig. 7b above 5 Hz. The rise of coherence at higher frequencies is probably due to phase coherent noise on the acceleration and induced pressure signals, possibly caused by vibration of the follower mount and attached pressure transducer and resistance wires.

Thus, the first step in the correction procedure was to cancel the effect of the acceleration of the air column a_z on the measured pressure p_m:

$$p_m = p_s - p_r, \tag{8}$$

where the subscripts s and r denote pressure on the signal and reference sides of the differential pressure transducer diaphragm. In what follows F is the operator used to account for the frequency response of the Elliott probe (Fig. 5):

$$p_0 = p_m + 0.86F(\rho_a a_z L_1) + 0.14(\rho_a a_z L_1) + 0.14(\rho_a a_z L_2), \tag{9}$$

where the second and third terms on the right-hand side model the response of p_s to the acceleration, while the fourth term models the response of p_r to the acceleration. The last term is relatively small ($L_2 = 0.1$ m, while $L_1 = 1.28$ m and without phase shift, since the back-up volume was closed, and 0.14 is the empirical value seen in Fig. 6 for the closed-end configuration. The second and third terms combined use the Fig. 6 dependences to model the configuration with the Elliott probe at the end of the connecting tubes: at very high frequencies, the Elliott probe end works as a closed end and therefore the induced pressure approaches the $0.14(\rho_a a_z L_1)$ value, as no air leakage through Elliott orifices takes place at those frequencies; at very low frequencies the configuration works as an open-end configuration, and the two terms combined should provide $\rho_a a_z L_1$ induced pressure; and in between, the parameterized transfer function applies. The signs of the third and fourth terms are both positive because the transducer was mounted vertically between probe and back-up volume, being above the former and below the latter. Thus p_0 is the pressure the MKS pressure transducer would record in the absence of acceleration effects on the air columns. Consequently, we put p_0 through the inverse transfer function of the probe–tubing–transducer set F^{-1}, to obtain the pressure just outside the Elliott probe p_a:

$$p_a = F^{-1}(p_0). \tag{10}$$

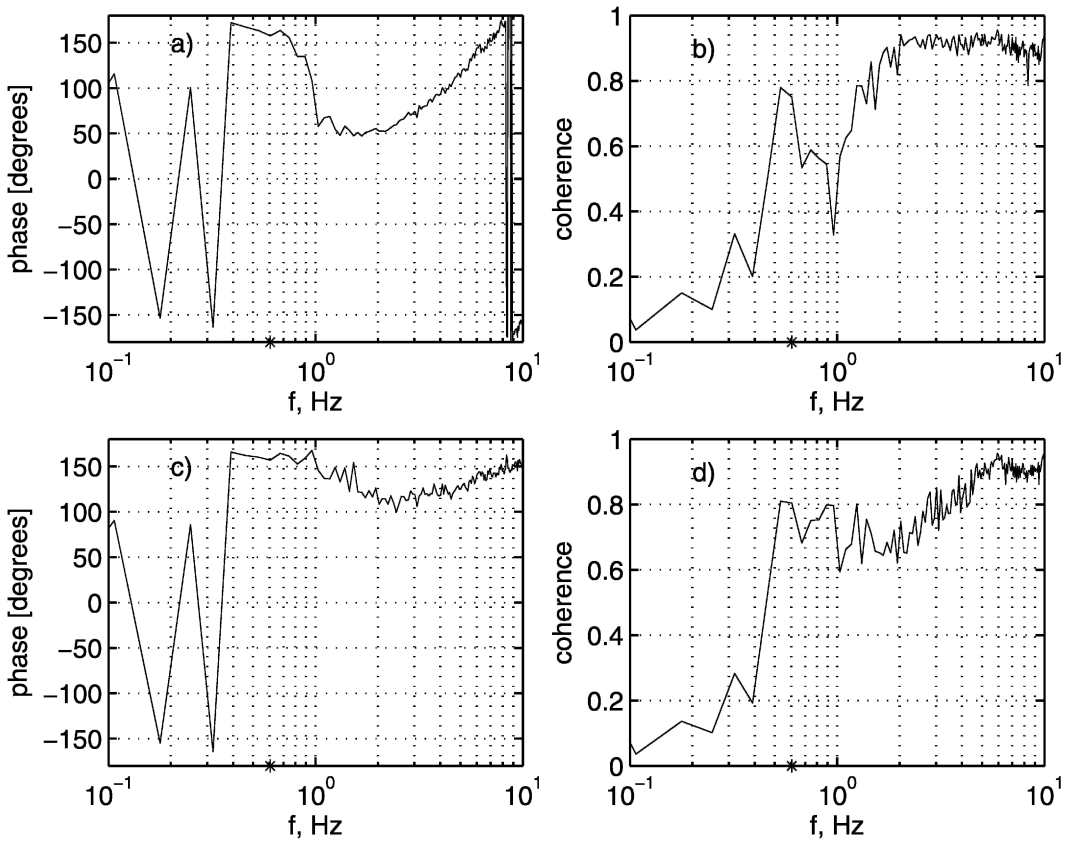

FIG. 7. (a), (c) Phase lag and (b), (d) coherence of a surface-elevation record and a synchronized Elliott-measured pressure signal, corrected for acceleration of the probe: (a), (b) pressure is assumed to be directly proportional to acceleration; (c), (d) the correction is frequency dependent, as in Fig. 6. Positive phase lag means the surface leads the pressure. Asterisks (*) mark the positions of the spectral peaks.

3) CORRECTION FOR THE STAGE DISPLACEMENT

The final correction to be performed on the recorded pressure signal is that due to the stage displacement in the vertical atmospheric pressure gradient. This stage displacement imposed pressure is

$$p_d = -\rho_a g z. \tag{11}$$

In principle, this pressure term is in antiphase with the surface elevation and therefore does not contribute to the quadrature spectrum. However, if there is a delay of the stage position reaction relative to the measured surface elevation, z, even though it is small (Fig. 4, phase shift subplot), then there will be leakage into the quadrature spectrum of surface elevation and pressure. The inverse of the transfer function of the stage (Fig. 4) was applied to the observed surface elevation to recover the stage position, z, before the corrections for z and $\ddot{z}$ were applied. (The comments made in this paragraph apply to all the acceleration corrections, since they, too, contribute mostly to the pressure–wave height spectrum.)

Thus, the real pressure at the entrance of the Elliott probe orifices is

$$p = p_a - p_d = p_a + \rho_a g z. \tag{12}$$

c. Removing the alias and spikes

To avoid aliasing, particularly for signals whose spectral densities do not fall off rapidly at higher frequencies, an electronic 10-Hz low-pass filter was applied to all the wave-follower analog channels. Prior to the data analysis, a numerical routine was applied to correct for the one-pole RC 10-Hz antialiasing filter transfer function. The electronic filtering was not applied to the stage position signal because it is a digital measuring device (stepping motor) and is recorded digitally.

Occasionally spikes would appear in the recorded signals, due to water droplets, electronic noise, and other reasons. The spikes have the potential to contaminate spectra and raise the noise level at higher frequencies. Thorough spike removal procedures were applied to all the time series prior to all the other correc-

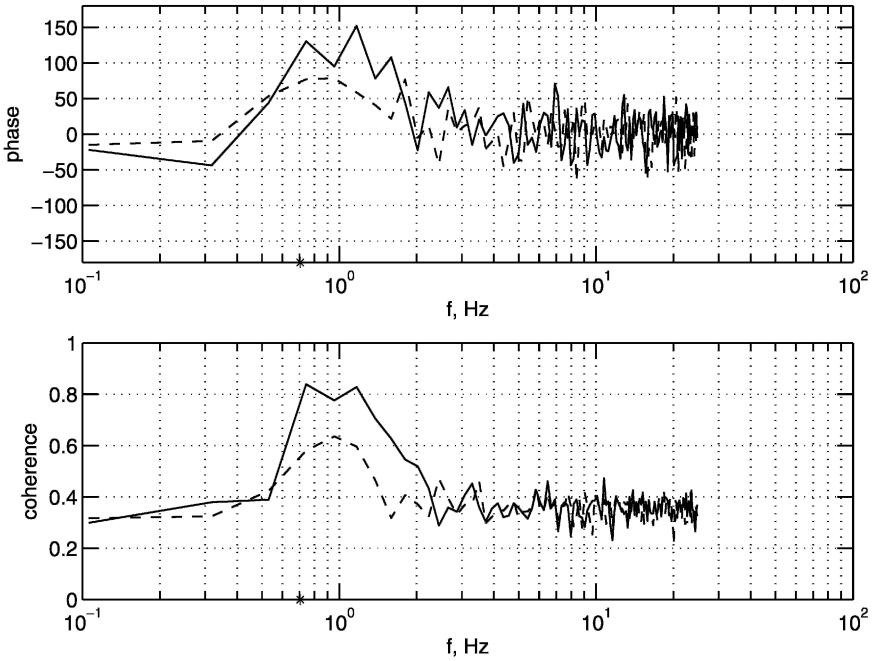

FIG. 8. (top) Phase lag and (bottom) coherence of a surface-elevation record with a corrected synchronized Elliott-measured pressure signal (solid line) and a hot-film vertical velocity (dashed line). Asterisks (*) mark the positions of the spectral peaks.

tions, based on two criteria: the signal was not to exceed a predetermined level of six standard deviations away from its mean and the first difference of the signal was not to exceed a predetermined threshold of 10 times the mean difference between consecutive samples.

d. Using Pitot tubes and hot films to verify the pressure data and wind-input results

The hot film and Pitot tube were positioned 10 and 15 cm, respectively, above the Elliott disk. They were farther from the water surface (Fig. 3b) than the Elliott probe, and therefore the frequency resolution of the wave-induced fluctuations in the air was a priori reduced compared to the Elliott probe. In fact, the Pitot tube signal, related to the horizontal velocities, was not coherent with the surface elevations in the entire frequency band of interest, including the wave spectrum peak region, if processed by means of conventional spectral analysis (coherent signals were recovered by a phase-averaging analysis procedure). The Pitot tube was used as an independent means to verify the pressure measurements by the Elliott probe.

The hot-film probes measured two-dimensional wind pulsations: the horizontal in line with the mean wind component and the vertical component. The wave-induced vertical velocity oscillations are linked with the induced pressure, and therefore the velocity oscillations, which are coherent with the surface, should exhibit behavior similar to that of the pressure fluctuations, though diminished due to the higher elevation of the velocity probe above the wavy surface. Indeed, the hot-film signal related to the vertical velocities had significant coherence with the surface, at least for the wave spectral peak frequencies. An example of phase and coherence frequency dependence, recorded in a fixed mode for both the Elliott pressure and hot-film vertical velocity component, is shown in Fig. 8. The Elliott probe was located 14 cm above the mean water level, which places the hot film almost twice as high, at 24 cm. As one could expect at such difference in heights, coherence of the hot-film vertical velocity signal with the surface elevations, compared to the pressure-to-surface coherence, is lower even at the spectral peak of $f_p = 0.71$ Hz and quickly drops below the significant level of 0.5 at higher frequencies. The phase shift exhibits similar behavior at the frequencies of significant coherence with the difference that the vertical velocity is in quadrature with the surface elevation, while the pressure is closer to being in antiphase with elevation.

As mentioned above, two hot-film probes were located on the wave follower: one on the moving arm, and a stationary pair on the body of the follower 1.5–1.7 m above the water surface (depending on the varying

water depth). The hot-film records enabled us to obtain variations of the local stresses very close to the surface in conjunction with other wind and wave properties and to estimate mean momentum fluxes. The latter served as a particularly important independent check of the integral of the measured momentum input spectra, as will be shown in Donelan et al. (2005, manuscript submitted to *J. Phys. Oceanogr.,* hereafter Part II). The hot films were calibrated in the wind tunnel of the Commonwealth Scientific and Industrial Research Organization (CSIRO), Canberra, Australia, just prior to AUSWEX, and the cup anemometers were calibrated at the wind tunnel of the School of Aerospace and Mechanical Engineering, Australian Defence Force Academy (ADFA), Canberra, immediately after AUSWEX. During the calibrations, both the hot wires and cup anemometers were held in a fixed position while a series of runs with stepped wind speeds was made. The calibration of the sonic anemometer was checked by the manufacturer in 1998 and is not subject to noticeable drift.

e. The bottom-pressure probes

Three bottom-pressure probes were installed in the water, on the bottom plate of the wave follower. The centroid of this triangle lay directly below the spot where the pressure was sensed at the surface. The probes proved to be very useful for multipurpose applications.

The bottom-pressure sensors were arranged as a triangle with the apex facing the same direction as the other probes (i.e., the direction of incoming waves and the wind) with 10-cm base. This allows one to obtain directional spectra locally and provides redundancy with the local array of three capacitance gauges. Since the water depth above the pressure probes was only 20–40 cm, a running correction for the changing depth due to passing waves was needed. The highly temporally resolved wavelet directional method (WDM) developed by Donelan et al. (1996) was used for this purpose.

A very important use of the bottom pressure probes was to indicate breaking events. In Part III of this paper, enhancement of the wind input above the breaking waves will be investigated, and therefore reliable and synchronous detection of the breakers was needed. The breaking waves generate acoustic pressure and enhanced pressure at high frequencies, which was sensed clearly by the collocated hydrophone (see Babanin et al. 2001). The same pressure was also detected by the pressure probes. Successful detection of the breaking events by the probes was verified with the synchronized video records and subsequently used for routine analysis of the wind-input enhancement. An HTI-96-MIN hydrophone (High Tech, Inc., Massachusetts), located on the bottom directly beneath the sensing spot of the Elliott probe and having its sensitive diaphragm exposed to downward propagating sound, was also used for these purposes.

Another application of the bottom-pressure probes was the determination of accurate water depths. Knowledge of the precise depth and therefore the Elliott probe altitude, which was measured relative to the lake's bottom, is a crucial point for the study, since the measured pressure fluctuations had to be accurately extrapolated to the surface by means of a yet unknown pressure altitude dependence. The water depth of the shallow Lake George changed due to wind setup and long-period seiches and had to be determined for each individual record. For this purpose, the bottom-pressure transducers were calibrated on a regular basis (a few times per day) and bottom-pressure running-average values were used, cross-checked with readings of the capacitance and resistance wave probes, to determine the water level and, together with the records of stage position, to determine the Elliott probe altitude.

f. Wave spectra and pressure-to-surface phase and coherence

As is mentioned in the beginning of this section, pressure in quadrature with the water surface [Eq. (2)] results in an energy flux from wind to waves. Therefore, the pressure-to-surface cross-spectrum is the primary objective of the experiment, and the phase shift of the local pressure relative to the local surface elevation carries very important information on the rate of the energy exchange.

An example of the phase shift and coherence spectra, together with the local wave power spectrum and energy input spectrum, is shown in Fig. 9. Confidence limits of spectral estimates of all the frequency distributions are very small. The error of the estimates, however, is determined by the whole set of measurement, calibration, transfer function, spectral analysis, and other correction errors and is impossible to evaluate in absolute values. Verification of the correctness of the measurements can be done by comparing the integral of the momentum input spectrum, resulting from the Elliott probe measurements, with the independently measured total wind stress by hot wires. Results of such comparisons will be shown in Part II.

This is a strongly wind forced situation, like most of the Lake George records, with $U_{10}/c_p = 4.2$, and it can be seen in the bottom spectra in Fig. 9 that a major part of the wind input is, in the spectral sense, concentrated

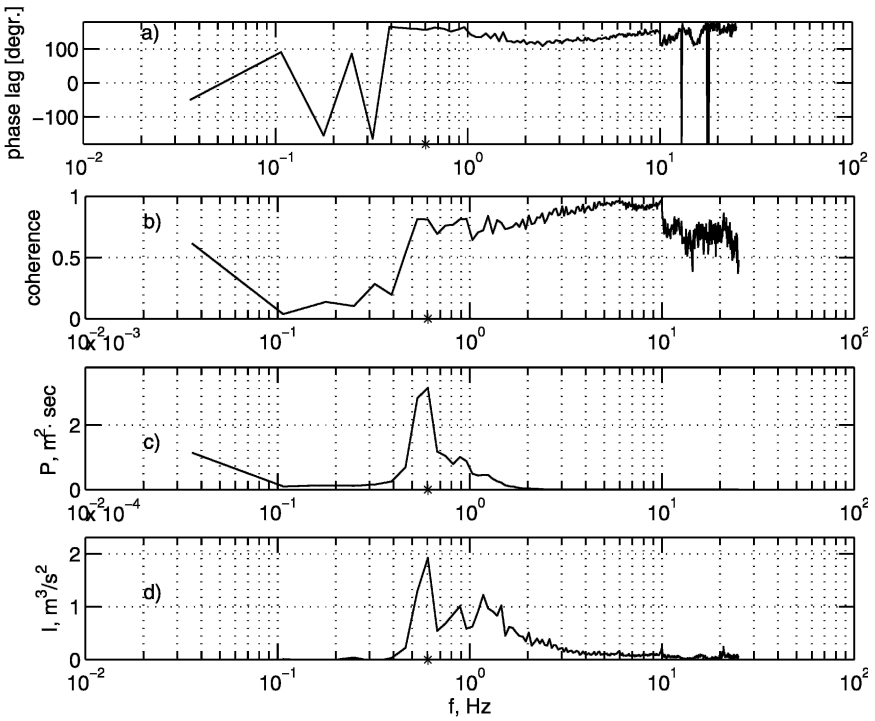

FIG. 9. (a) Phase lag and (b) coherence of synchronized surface-elevation and pressure records. (c) Wave power spectrum of the record. (d) Energy wind-input spectrum. Asterisks (*) mark the positions of the spectral peaks.

near the dominant waves. The phase shift between the surface and the pressure (top spectrum) is different from potential theory (180°), and this difference provides the effective mechanism for pumping energy from the wind into the waves. The physical features of the energy exchange mechanism will be discussed in detail in Part II.

4. Conclusions

This paper presents the technical aspects of a wind-input study carried out at Lake George, Australia, during the Australian Shallow Water Experiment (AUSWEX). Obtaining field measurements of the wind input to waves is a complex and demanding task, attempted only a few times previously. The AUSWEX technical solution to the problem involved a new level of precision of wave-following measurements. In the present study, conducted in field conditions, the wave-induced pressure oscillations were measured up to 4-Hz frequency, with a potential of resolving 6-Hz wave-coherent pressure. In other field studies employing wave followers (Snyder et al. 1981; Hsiao and Shemdin 1983), the frequency resolution was limited by an upper bound of 0.7–0.8 Hz (the limit was inferred from figures and tables in the respective papers). Even more accurate laboratory wave-following measurements by Young and Sobey (1985) and Donelan (1999) were limited to 1–2 Hz in frequency.

A multifaceted approach to the measurements, which allowed independent, sometimes multiple, backup systems and verifications of important measured properties, was adopted. Thorough calibrations and signal corrections, some of which were inferred and performed for the first time, were also applied. Also, for the first time, synchronous detection of wave-breaking events was conducted since the influence of breakers on the momentum exchange process was one of the ideas being tested in this project.

To measure microscale oscillations of induced pressure above surface waves, a high-precision wave-follower system was developed at the University of Miami, Florida. The principal sensing hardware included Elliott probes, hot x-films, and Pitot tubes. The wave-follower recordings were supplemented by a complete set of relevant measurements in the atmospheric boundary layer, on the surface and in the water body. The arrangement of the field experiment, the instrumentation, the measurement procedure, and the data processing were addressed in detail.

It was demonstrated that the precision of the wave-following mechanism was sufficient to obtain the re-

quired measurement accuracy in the relevant range of wave heights and frequencies, up to 4 Hz. We have described the calibration procedure for the pressure transducer and multiple corrections to the sensed pressure: correction for acceleration of the pressure sensor and the tubing that connected the sensor and the transducer; correction for the stage displacement in the boundary layer; correction for the pressure response in the backup volume; and removing the low-pass-filtering effect of the probe–tubing–transducer system in order to recover the original pressure at the entrance of the Elliott probe orifices. It was shown for the first time that a frequency-dependent correction is needed to account for the acceleration of the probe and tubes. The acceleration correction, routinely used in previous experiments and proportional to the second derivative of stage displacement, leads to significant contamination of the pressure signal and distortion of the resultant wind-input term.

We have discussed methods of alternative verification of the measured values and spectra, methods of synchronous detection of breaking waves, and methods of accurate recovery of water depths and following probe heights.

Acknowledgments. The authors gratefully acknowledge the financial support of the U.S. Office of Naval Research (Grants N00014-97-1-0234 and N00014-97-1-0233) and the Australian Research Council (Grant A00102965). We also express our gratitude to the staff of the School of Civil Engineering of the Australian Defence Force Academy for their help during AUSWEX, particularly Michael Jones, Mary Dalton, and John MacLeod, who offered highly professional and prompt responses to all urgent demands during the experiment. We are also very grateful to CSIRO, Canberra, and the School of Aerospace and Mechanical Engineering, ADFA, for their assistance with calibrations of the wind probes. We thank our colleague, Fred Dobson, and the two referees for many constructive comments that greatly added to the clarity and precision of this paper.

REFERENCES

Babanin, A. V., I. R. Young, and M. L. Banner, 2001: Breaking probabilities for dominant surface waves on water of finite constant depth. *J. Geophys. Res.,* **106,** 11 659–11 676.

Banner, M. L., 1990: The influence of wave breaking on the surface pressure distribution in wind–wave interactions. *J. Fluid Mech.,* **211,** 463–495.

——, and W. K. Melville, 1976: On the separation of air flow above water waves. *J. Fluid Mech.,* **77,** 825–842.

Dobson, F. W., 1971: Measurements of atmospheric pressure on wind-generated sea waves. *J. Fluid Mech.,* **27,** 91–127.

Donelan, M. A., 1999: Wind-induced growth and attenuation of laboratory waves. *Wind-over-Wave Couplings: Perspective and Prospects,* S. G. Sajadi, N. H. Thomas and J. C. R. Hunt, Eds., Clarendon Press, 183–194.

——, W. M. Drennan, and A. K. Magnusson, 1996: Nonstationary analysis of the directional properties of propagating waves. *J. Phys. Oceanogr.,* **30,** 3145–3160.

——, N. Madsen, K. K. Kahma, I. K. Tsanis, and W. M. Drennan, 1999: Apparatus for atmospheric surface layer measurements over waves. *J. Atmos. Oceanic Technol.,* **16,** 1172–1182.

Elliott, J. A., 1972a: Instrumentation for measuring static pressure fluctuations within the atmospheric boundary layer. *Bound.-Layer Meteor.,* **22,** 476–495.

——, 1972b: Microscale pressure fluctuations near waves being generated by wind. *J. Fluid Mech.,* **54,** 427–448.

Hasselmann, D., and J. Bösenberg, 1991: Field measurements of wave-induced pressure over wind-sea and swell. *J. Fluid Mech.,* **230,** 391–428.

Hasselmann, K., 1960: Grundleiehungen der Seegangsvoraussage. *Schiffstechnik,* **7,** 191–195.

Hsiao, S. V., and O. H. Shemdin, 1983: Measurements of wind velocity and pressure with a wave follower during MARSEN. *J. Geophys. Res.,* **88,** 9841–9849.

Longuet-Higgins, M. S., D. E. Cartwright, and N. D. Smith, 1963: Observation of the directional spectrum of sea waves using the motions of a floating buoy. *Ocean Wave Spectra: Proceedings of the Conference on Ocean Wave Spectra,* Prentice Hall, 111–136.

Plant, W. J., 1982: A relationship between wind stress and wave slope. *J. Geophys. Res.,* **87,** 1961–1967.

Snyder, R. L., 1974: A field study of wave-induced pressure fluctuations above surface gravity waves. *J. Mar. Res.,* **24,** 141–178.

——, F. W. Dobson, J. A. Elliott, and R. B. Long, 1981: Array measurements of atmospheric pressure fluctuations above surface gravity waves. *J. Fluid Mech.,* **102,** 1–59.

Sobey, R. J., 1986: Wind-wave prediction. *Annu. Rev. Fluid Mech.,* **16,** 149–172.

Veron, F., and W. K. Melville, 1999: Pulse-to-pulse coherent Doppler measurements of waves and turbulence. *J. Atmos. Oceanic Technol.,* **16,** 1580–1597.

Young, I. R., 1999: *Wind Generated Ocean Waves.* Elsevier, 288 pp.

——, and R. J. Sobey, 1985: Measurements of the wind-wave energy flux in an opposing wind. *J. Fluid Mech.,* **123,** 427–442.

——, and L. A. Verhagen, 1996a: The growth of fetch limited waves in water of finite depth, Part I: Total energy and peak frequency. *Coastal Eng.,* **29,** 47–78.

——, and ——, 1996b: The growth of fetch limited waves in water of finite depth, Part II: Spectral evolution. *Coastal Eng.,* **29,** 79–100.